Asymmetric Supercapacitors Using 3D Nanoporous Carbon and Cobalt Oxide Electrodes Synthesized from a Single Metal–Organic Framework

Rahul R. Salunkhe,[†] Jing Tang,[†,‡] Yuichiro Kamachi,[†,§] Teruyuki Nakato,[§] Jung Ho Kim,*[,∥] and Yusuke Yamauchi*[,†,‡]

[†]World Premier International (WPI) Research Center for Materials Nanoarchitectonics (MANA), National Institute for Materials Science (NIMS), 1-1 Namiki, Tsukuba, Ibaraki 305-0044, Japan, [‡]Faculty of Science and Engineering, Waseda University, 3-4-1 Okubo, Shinjuku, Tokyo 169-8555, Japan, [§]Department of Applied Chemistry, Graduate School of Engineering, Kyushu Institute of Technology, 1-1 Sensui-Cho, Tobata, Kitakyushu, Fukuoka 804-8550, Japan, and [∥]Institute for Superconducting and Electronic Materials, University of Wollongong, North Wollongong, New South Wales 2500, Australia

ABSTRACT Nanoporous carbon and nanoporous cobalt oxide (Co_3O_4) materials have been selectively prepared from a single metal–organic framework (MOF) (zeolitic imidazolate framework, ZIF-67) by optimizing the annealing conditions. The resulting ZIF-derived carbon possesses highly graphitic walls and a high specific surface area of 350 $m^2 \cdot g^{-1}$, while the resulting ZIF-derived nanoporous Co_3O_4 possesses a high specific surface area of 148 $m^2 \cdot g^{-1}$ with much less carbon content (1.7 at%). When nanoporous carbon and nanoporous Co_3O_4 were tested as electrode materials for supercapacitor application, they showed high capacitance values (272 and 504 $F \cdot g^{-1}$, respectively, at a scan rate of 5 $mV \cdot s^{-1}$). To further demonstrate the advantages of our ZIF-derived nanoporous materials, symmetric (SSCs) and asymmetric supercapacitors (ASCs) were also fabricated using nanoporous carbon and nanoporous Co_3O_4 electrodes. Improved capacitance performance was successfully realized for the ASC (Co_3O_4//carbon), better than those of the SSCs based on nanoporous carbon and nanoporous Co_3O_4 materials (*i.e.*, carbon//carbon and Co_3O_4//Co_3O_4). The developed ASC with an optimal mass loading can be operated within a wide potential window of 0.0–1.6 V, which leads to a high specific energy of 36 $W \cdot h \cdot kg^{-1}$. More interestingly, this ASC also exhibits excellent rate capability (with the highest specific power of 8000 $W \cdot kg^{-1}$ at a specific energy of 15 $W \cdot h \cdot kg^{-1}$) combined with long-term stability up to 2000 cycles.

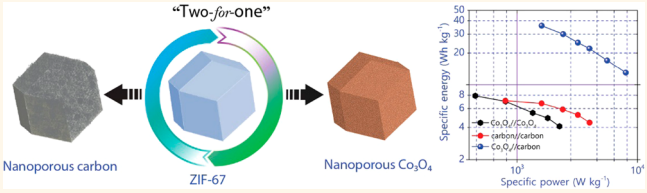

KEYWORDS: nanoporous materials · coordination polymers · metal–organic frameworks · cobalt oxide · carbon · supercapacitors

The rapid increase in world population and hike in the economic expansion around the world have led to increasing use of energy-based appliances, which eventually results in high energy consumption.[1−3] As a consequence, great research efforts have been made toward the development of energy conversion and storage. At present, batteries and electrochemical capacitors (ECs) play important roles as leading electrical energy storage (EES) devices. Although lithium-ion batteries for consumer electronics have made substantial advances,[4] ECs also possess some very attractive properties, such as higher power density than batteries (~10 000 $W \cdot kg^{-1}$), short charging time (on the order of tens of seconds), and long cycle life over repeated charge–discharge (>100 000 cycles), which makes them promising candidates for various applications such as for frequency regulation in smart grids, hybrid electric vehicles, *etc.*[5,6] Nevertheless, energy density is a crucial factor for ECs (carbon-based EC[7,8] is ~10 $W \cdot h \cdot kg^{-1}$, and EC based on asymmetric configuration[9,10] is ~30 $W \cdot h \cdot kg^{-1}$), which limits their comprehensive use.

Based on their charge storage mechanism, ECs can be mainly divided into two categories. The first is based on the charge-transfer Faradaic reaction (pseudocapacitance),[11,12] and the second is electrical double-layer capacitance (EDLC),[13,14] which is a non-Faradaic process. Comparatively, the pseudocapacitance mechanism, which is based on transition metal oxides, has advantages such as typically

* Address correspondence to jhk@uow.edu.au, Yamauchi.Yusuke@nims.go.jp.

Received for review March 24, 2015 and accepted May 15, 2015.

Published online May 15, 2015
10.1021/acsnano.5b01790

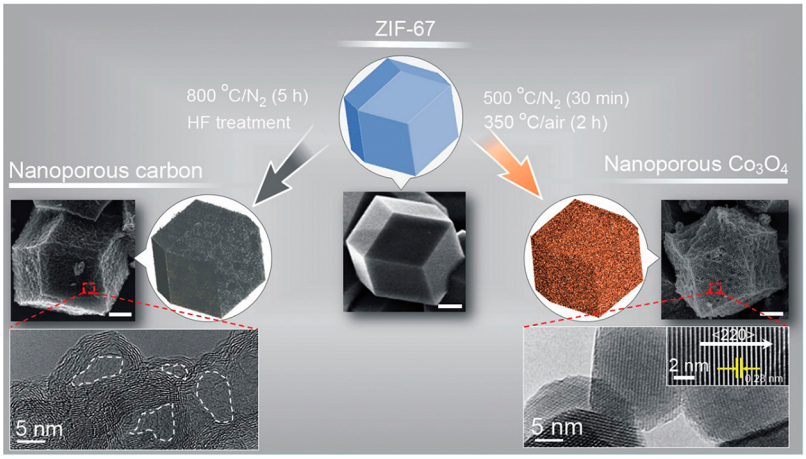

Scheme 1. Schematic illustration of the preparation process of nanoporous carbon and nanoporous Co_3O_4 from a ZIF-67 polyhedron as the single precursor by optimized thermal treatment. The actual SEM images and high-resolution TEM images of the respective materials are as shown below their illustrations. The scale bars shown in the SEM images are 500 nm in length. More detailed TEM analysis suggests that, after the thermal treatment and HF washing, nanopores are formed on the nanoporous carbon surface (as shown by dotted lines) due to the removal of cobalt nanoparticles, whereas in the case of Co_3O_4, the optimized heating conditions result in conversion of the ZIF-67 polyhedron into an oxide polyhedron with granular particles on the polyhedron surface.

high capacitance (up to 1000 $F \cdot g^{-1}$),[15,16] which leads to better energy density than in EDLC-type capacitors. So far, many reports have appeared in the literature on the development of different metal oxides for supercapacitor applications.[17−21] Although various methods for morphological and structural control of metal oxides have been demonstrated in recent research efforts, a simple synthesis strategy for the development of porous three-dimensional (3D) metal oxides is still a challenge. Porous metal oxides with controlled porosity often exhibit physical properties that are different from those of bulk materials.[22,23] Thus, the control of porosity, morphology, and surface area will lead to the development of a new era of material synthesis that will be useful for next-generation energy storage.

Among the many metal oxides, cobalt oxide materials can be considered as superior materials for supercapacitor applications, due to fact that they have high theoretical capacitance values (~3600 $F \cdot g^{-1}$), low cost, environmental friendliness, high electrochemical stability, *etc.*[24,25] Numerous methods have been reported for the synthesis of Co_3O_4 with controlled microstructure in one-dimensional[25−29] and two-dimensional[30−32] form. More importantly, some of these reported methods are well-optimized chemical routes that require control of two or more parameters during the preparation, which adds uncertainty about morphological control and reproducibility on a large scale.

To date, many reports are available in the literature on the development of asymmetric supercapacitors (ASCs),[9,10] which are based on the development of a positive electrode only (basically, metal oxides).[9−11] In most cases, activated carbon (AC) or stacked graphene has been used as the negative electrode. Nevertheless, a key problem is that the asymmetric performance not only is limited to the positive electrode but also requires a contribution from the negative electrode. Thus, a challenging problem for high-performance ASCs is the development of both positive and negative materials by a simple synthesis method with controlled porosity and shapes that can be easily tuned.

An important frontier in material synthesis is the development of two kinds of materials from a single precursor. This idea of "*two-for-one*" has been recognized in other solid materials; however, the ability to tune their compositions without changing their original shapes has not been achieved yet. Metal−organic frameworks (MOFs) are materials with high surface area and high porosity that have been mostly used for gas adsorption[33] and catalysis[34] applications but still remain unexplored in the area of EES devices such as supercapacitors. MOFs can be easily and selectively converted into their respective metal oxides, metal sulfides, or carbons by changing the thermal conditions.[35−45] Such MOF-derived nanoporous metal oxides and carbons have high surface area and interconnected pores,[46,47] which are useful for improved performance in several applications.[48,49] Thus, the MOF represents a new approach for the development of smart materials, requiring the development of two materials from one precursor.

In the present study, we have selected the ZIF-67 single precursor for preparation of nanoporous carbon and nanoporous cobalt oxides (Co_3O_4). Then, we demonstrate the development of an ASC based on MOF-derived nanoporous carbon and Co_3O_4 electrodes. By coupling the advantages of a positive electrode, consisting of pseudocapacitive Co_3O_4 with high surface area, and a negative electrode, consisting of EDLC carbon, this novel ASC gives a high energy density value of 36 $W \cdot h \cdot kg^{-1}$. The energy density

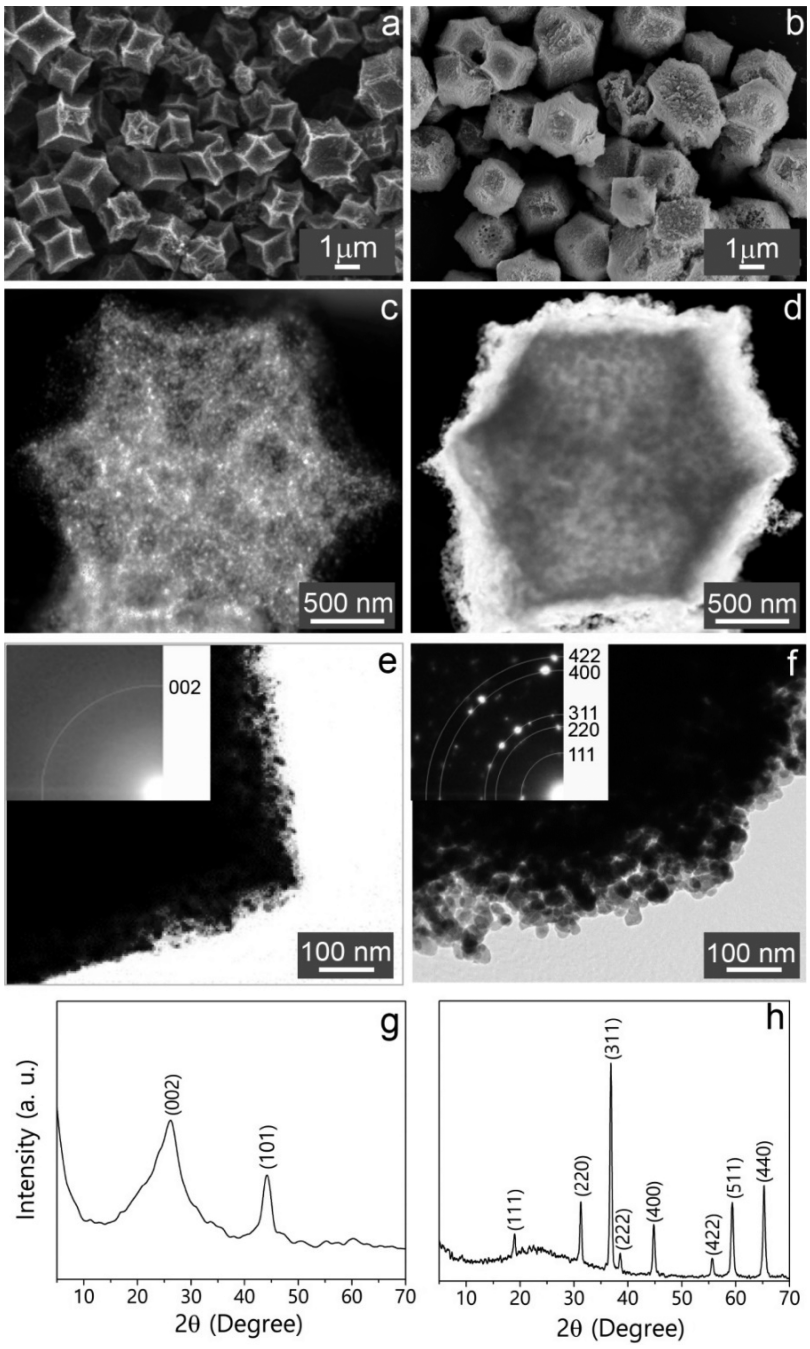

Figure 1. (a,b) SEM images, (c,d) high-angle annular dark-field scanning transmission electron microscope (HAADF-STEM) images, (e,f) bright-field TEM images, and (g,h) wide-angle XRD patterns of (a,c,e,g) nanoporous carbon and (b,d,f,h) nanoporous Co_3O_4. Insets of (e,f) show SAED patterns of (e) nanoporous carbon and (f) nanoporous Co_3O_4.

obtained from this asymmetric supercapacitor (Co_3O_4//carbon) is much higher than those for symmetric supercapacitor (SSC) configurations (*i.e.*, carbon//carbon and Co_3O_4//Co_3O_4).

RESULTS AND DISCUSSION

Material Characterization. Details of the synthetic method for the nanoporous carbon and Co_3O_4 are illustrated in Scheme 1. ZIF-67 crystals were prepared by a simple reaction of 2-methylimidazole with cobalt ions. The details are given in the Experimental Methods section. The obtained ZIF-67 crystals were characterized by wide-angle X-ray diffraction (XRD), and the pattern shows a typical ZIF-67 crystal (Figure S1 in the Supporting Information). The carbonization of ZIF-67 at 800 °C gives nanoporous carbon, although it contains some Co nanoparticles, which can be removed by acid treatment. For the preparation of nanoporous Co_3O_4, in order to retain the original polyhedral shape, we have preheated the ZIF-67 crystals in nitrogen. Such a preheating treatment can realize good retention of the original shape by the Co_3O_4 polyhedra.

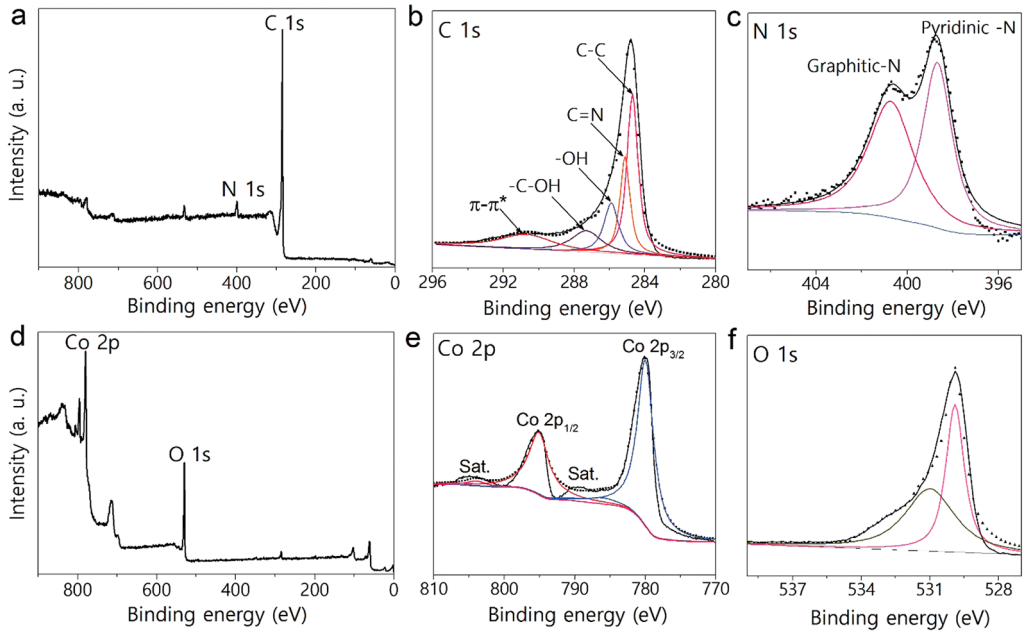

Figure 2. XPS survey spectra for (a) nanoporous carbon and (d) nanoporous Co_3O_4. XPS spectra for (b) C 1s, (c) N 1s, (e) Co 2p, and (f) O 1s.

The surface morphology of the nanoporous carbon and Co_3O_4 was characterized by using scanning electron microscopy (SEM) and transmission electron microscopy (TEM). From the low-magnification SEM images (Figure 1a,b), it can be clearly observed that the polyhedral shape of the ZIF-67 precursor is well retained by the nanoporous carbon and Co_3O_4. For the nanoporous Co_3O_4, Co_3O_4 nanocrystals with an average size of 15−20 nm can be clearly observed on the surfaces of the polyhedra (Figure 1d,f). Similar types of granular structures are observed for different MOF-derived metal oxides.[35,41] The selected area electron diffraction (SAED) patterns (inset of Figure 1f) clearly show the formation of rings, which can be indexed to the (111), (220), (311), (400), and (422) planes of Co_3O_4 (JCPDs card 42-1467). As can be seen in Scheme 1, the interplanar spacing of the crystalline grains was calculated to be 0.28 nm, corresponding to the (220) plane orientation. On the other hand, the nanoporous carbon shows a rough surface due to the formation of nanopores (Figure 1c,e). The high-resolution TEM image clearly shows the presence of several pores (as indicated by dotted lines in Scheme 1), which are formed after the removal of Co nanoparticles by HF washing.[50] The SAED pattern (inset of Figure 1e) shows partially graphitized walls. The powder XRD pattern of nanoporous carbon shows the presence of two broad peaks from the (002) and (101) planes (Figure 1g), suggesting the formation of graphitic carbon (sp^2-bonded carbon).[50] In the case of nanoporous Co_3O_4 (Figure 1h), all the diffraction patterns can be assigned to cubic phase Co_3O_4 (JCPDs card number 42-1467).

The chemical compositions of the nanoporous carbon and Co_3O_4 were analyzed by energy-dispersive X-ray spectroscopy. Both materials were examined for selected elements, namely, carbon, cobalt, oxygen, and nitrogen, as summarized in Figure S2. Nanoporous carbon contains negligible cobalt content, while nanoporous Co_3O_4 contains negligible carbon content.

The porosity of the samples was characterized by nitrogen adsorption−desorption isotherms (Figure S3a,c). The Brunauer−Emmett−Teller (BET) specific surface area obtained for nanoporous carbon was 350 $m^2 \cdot g^{-1}$, whereas the pore size distribution obtained from the Barrett−Joyner−Halenda method revealed two narrow distributions centered at 3 and 5−15 nm (Figure S3b). The pore size distribution clearly reveals that the nitrogen adsorption by the micropores is much higher than that of mesopores. In the case of nanoporous Co_3O_4, a high BET specific surface area (148 $m^2 \cdot g^{-1}$) was obtained, which is much higher than that for the previously reported Co_3O_4 nanostructures.[26,27,30,31,51,52] Direct comparisons of the surface area of our Co_3O_4 polyhedral nanostructures with previously reported Co_3O_4 nanostructures, produced by various synthetic routes, are summarized in Table S1. To the best of our knowledge, our value is the highest surface area among all the previous reports based on Co_3O_4 nanostructures, which clearly highlights the advantage of our method. The pore size distribution indicates that the majority of pores are in the mesoporous region (Figure S3d). The high specific surface area provides more reaction sites for electrochemical interactions/reactions, which are beneficial for supercapacitor applications.

More detailed analysis was carried out using X-ray photoelectron spectroscopy (XPS) (Figure 2). The C 1s spectrum for nanoporous carbon presented in Figure 2b can be deconvoluted into five major peaks.[50] The peak at 284.6 eV corresponds to the C−C bonds of

TABLE 1. Compositional Ratios of Cobalt, Oxygen, Carbon, and Nitrogen in Nanoporous Carbon and Co_3O_4 Samples[a]

materials	Co (at%)	O (at%)	C (at%)	N (at%)
nanoporous carbon	1.4	2.7	90.8	5.1
nanoporous Co_3O_4	36.9	57.4	1.7	4

[a] The ratios are calculated by XPS analysis.

sp^3-carbon. The peak at 285.1 eV is assigned to the sp^2-carbon containing nitrogen atoms (C═N bond). The carbon atoms bonded to hydroxyl groups (−OH) and carbonyl groups (−C═O) are represented by peaks at 285.9 and 287.3 eV, respectively. A small peak at 290.7 eV can be assigned to $\pi-\pi^*$ electronic transitions.[53] The nitrogen (N 1s) spectra (Figure 2c) can be mainly deconvoluted into two peaks with binding energies at 398.8 eV (pyridinic-N) and 400.8 eV (graphitic-N).[54] For nanoporous Co_3O_4, the XPS peak for Co 2p shows two major peaks with binding energies of 779.86 and 795.1 eV, corresponding to Co $2p_{3/2}$ and Co $2p_{1/2}$, which are characteristic peaks for the Co_3O_4 phase (Figure 2e). The two small peaks at 786 and 803.92 eV are typical Co^{2+} shakeup satellite peaks of Co_3O_4.[55] The energy difference between the Co $2p_{3/2}$ and Co $2p_{1/2}$ peaks is approximately 15 eV. The deconvoluted XPS spectra (Figure 2f) for O 1s display two types of contributions for oxygen species. One is the oxygen species corresponding to the spinel Co_3O_4 phase (529.96 eV),[55] and the other one indicates the presence of −OH species on the surfaces of nanostructured Co_3O_4 grains (531.1 eV).[30] The detailed compositions of cobalt, oxygen, carbon, and nitrogen in the nanoporous carbon and Co_3O_4 materials are summarized in Table 1.

Electrochemical Characterization of Nanoporous Carbon and Co_3O_4. The obtained nanoporous carbon and Co_3O_4 were tested as electrodes for supercapacitor applications. First, to evaluate the operating potential window and the charge on individual nanoporous carbon and Co_3O_4 electrodes, the electrodes were subjected to cyclic voltammetry (CV) using the standard three-electrode system in an aqueous KOH electrolyte (6 M). The CV studies for the nanoporous carbon electrodes (Figure 3a) were carried out in the potential window of −0.1 to −1.1 V (*vs* Ag/AgCl), while the CVs for the nanoporous Co_3O_4 electrodes (Figure 3b) were measured in the potential window of −0.1 to 0.4 V (*vs* Ag/AgCl). Various scan rates from 5 to 200 mV·s^{-1} were applied. In the case of nanoporous carbon, a semirectangular CV shape with a wide potential window of 1 V was observed. The specific capacitance values were 272, 211, 194, 186, 181, 176, 169, and 163 F·g^{-1} at the different scan rates of 5, 20, 40, 60, 80, 100, 150, and 200 mV·s^{-1}, respectively (Figure 3c). In the case of nanoporous Co_3O_4, a pair of redox peaks was observed due to the following reversible reaction of Co_3O_4 with OH^- anions.[56]

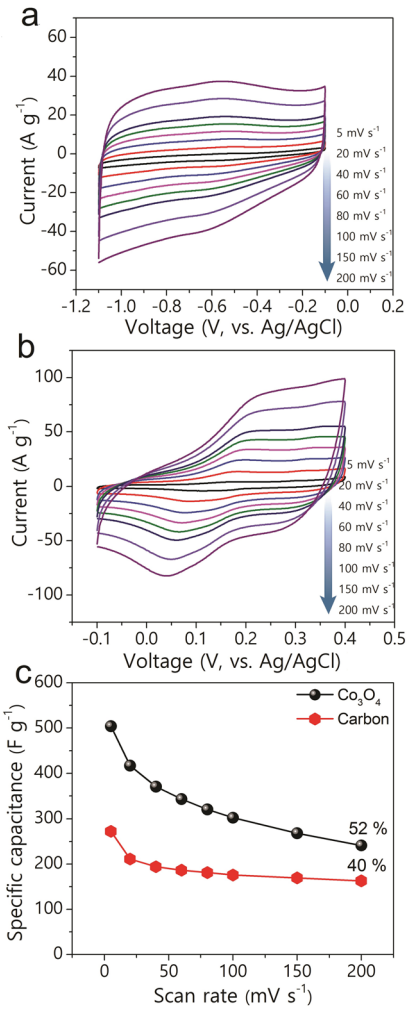

Figure 3. CV curves of (a) nanoporous carbon and (b) nanoporous Co_3O_4 at various scan rates from 5 to 200 mV·s^{-1}. (c) Scan rate dependence of specific capacitance for nanoporous carbon and nanoporous Co_3O_4 electrodes.

$$Co_3O_4 + OH^- + H_2O \leftrightarrow 3CoOOH + e^- \quad (1)$$

$$CoOOH + OH^- \leftrightarrow CoO_2 + H_2O + e^- \quad (2)$$

All the CV curves are mirror symmetric with good reversibility, indicating pseudocapacitive behavior of the Co_3O_4 electrode material. The specific capacitance values calculated from the CV curves (Figure 3c) were 504, 417, 371, 343, 320, 302, 268, and 241 F·g^{-1} at the different scan rates of 5, 20, 40, 60, 80, 100, 150, and 200 mV·s^{-1}, respectively. Thus, the 3D polyhedral porous structure provides very stable and symmetrical-shaped CVs, indicating improved capacitance performance compared with the previous reports available in the literature (Table S2).

ASC Study Based on Nanoporous Carbon and Co_3O_4. The capacitive performance of symmetric supercapacitors and asymmetric supercapacitors based on nanoporous carbon and Co_3O_4 were evaluated using CV

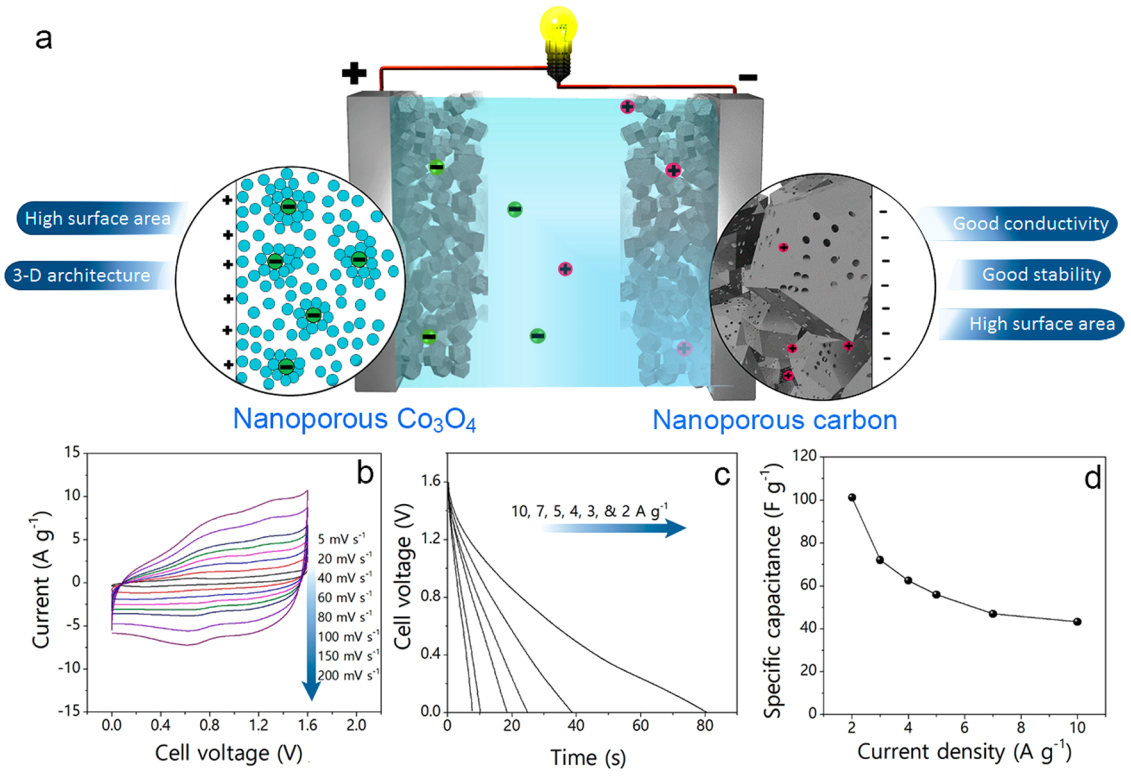

Figure 4. (a) Schematic illustration of ASC cell containing nanoporous Co_3O_4 and nanoporous carbon as the positive and negative electrodes, respectively. (b) CV curves of ASC. The device is cycled with a cell voltage from 0.0 to 1.6 V at various scan rates from 5 to 200 mV·s^{-1}. (c) Galvanostatic discharge curves of Co_3O_4//carbon ASC cell at various current densities from 2 to 10 A·g^{-1}. (d) Dependence of specific capacitance on the applied current density.

and galvanostatic charge−discharge (CD) methods. As can be seen from Figure 4a, the positive electrode of the ASC is Co_3O_4 with a granular morphology that provides easy access to a large number of ions to penetrate deep inside the porous material, which gives proper utilization of effective mass. On the other side, nanoporous carbon plays an effective role by providing fast charge transfer through its compatible pore structure. Thus, this specially designed ASC will link the advantages of these two materials to provide high specific energy and specific power. The performance of the ASC was evaluated using CV studies in different potential windows, as shown in Figure S4a. The CV curves are very rectangular and symmetric in shape, even though the potential window is extended up to 1.6 V, indicating ideal capacitive properties with good reversibility. After 1.6 V, however, there is a hump in the current, indicating that some irreversible chemical reactions occur above that potential. The rectangular CV shape is retained very well, even at the high scan rate of 200 mV·s^{-1}, suggesting that the ASC cell possesses high power capability (Figure 4b). Thus, this ASC can be operated within a wide potential window with a maximum working potential of 1.6 V. The detailed analysis of the SSCs in terms of the optimized potential window, galvanostatic charge−discharge curves, and capacitance variation with scan rate is presented in Figures S5 and S6.

The galvanostatic charge−discharge measurements were carried out at various current densities (Figure 4c). The specific capacitance value calculated at a current density of 2 A·g^{-1} was 101 F·g^{-1}, which only decreased to 43 F·g^{-1}, even at the high current density of 10 A·g^{-1}. The initial voltage loss (*i.e.*, *IR* drop) observed from the discharge curves is small, even at high current density, indicating a fast *I*−*V* response and low internal resistance of the supercapacitor.[9] The specific capacitance as a function of applied current density is plotted in Figure 4d. The specific capacitance values calculated at various current densities are 101, 72, 62, 58, 45, and 43 F·g^{-1} at different current densities of 2, 3, 4, 5, 7, and 10 A·g^{-1}, respectively.

Furthermore, a Ragone plot (specific power *vs* specific energy), which is a performance indicator for energy storage devices, was used to evaluate the performance of our ASC. Here, we fabricated two types of SSC cells (carbon//carbon and Co_3O_4//Co_3O_4) and one ASC cell (Co_3O_4//carbon) for comparison purposes (Figure 5a). It was found that the SSC based on carbon//carbon exhibits maximal specific energy of 7.1 W·h·kg^{-1} and specific power of 800 W·kg^{-1}, while the other SSC based on Co_3O_4//Co_3O_4 exhibits maximal specific energy of 7.9 W·h·kg^{-1} and specific power of 450 W·kg^{-1}. On the other hand, the ASC realizes both high specific energy of 36 W·h·kg^{-1} and high specific power of 1600 W·kg^{-1} at the current density of 2 A·g^{-1}.

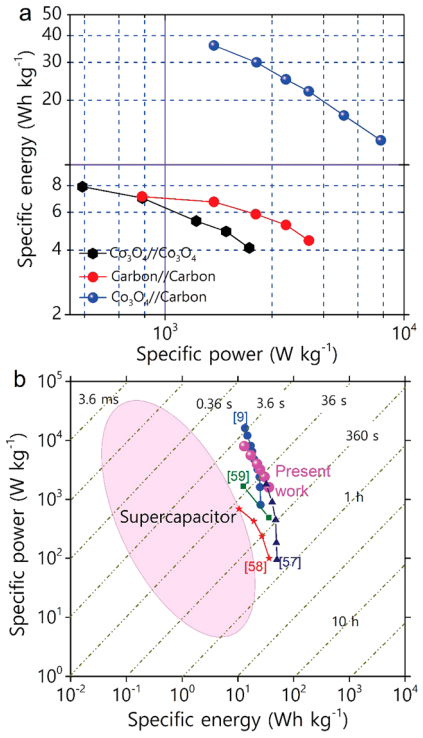

Figure 5. (a) Ragone plots of SSCs and ASC based on nanoporous carbon and nanoporous Co_3O_4 electrodes. (b) Comparison of our ASC full cell (Co_3O_4//carbon) with some reports in the literature.[9,57−59]

The specific energy and specific power change with the applied current density are summarized in Table S3. The values of specific energy obtained for the ASC are almost four times higher than those for the SSCs. Thus, the values obtained for specific energy and specific power for the ASC show improved performance.

It is obvious that the presence of a nanoporous and pseudocapacitive material such as Co_3O_4 helps in attaining higher current sweeps, whereas the nanoporous graphitic carbon is mainly responsible for providing a stable and wide potential window, which makes a major contribution to the high performance of the ASC. A comparison of the specific energy and specific power obtained from our ASC with those in previous reports is shown in Figure 5b. Even though when we compare our ASC performance with different metal oxides/hydroxides, our ASC shows comparable performance to the previous reports for specific energy without much sacrifice of specific power (Table S4). Life-cycle test was carried out using CD studies at a current density of 5 A·g^{-1} up to 2000 cycles (Figure S4b). The arbitrary chosen repeated CD cycles are shown in the inset of Figure S4b. Interestingly, these electrodes show a very promising performance up to 2000 cycles, with a slight decrease in capacitance of 11%. Thus, our results obtained in the present study have demonstrated a novel and efficient way to improve the specific energy, specific power, and rate capability of ASCs using MOF-derived nanoporous materials.

CONCLUSIONS

We have demonstrated a unique approach to an ASC application, in which both the electrode materials are derived from ZIF-67 as the single precursor source. The optimized conversion process for the preparation of nanoporous carbon and Co_3O_4 helps to retain the original polyhedral morphology of the original ZIF-67 crystals. This three-dimensional nanoporous structure provides a highly accessible surface area for electrochemical applications. Symmetric and asymmetric supercapacitors were fabricated by using nanoporous carbon and Co_3O_4 electrodes. The ASC (Co_3O_4//carbon) exhibited a high specific energy of 36 W·h·kg^{-1} and a high specific power of 8000 W·kg^{-1}, which were much higher than those for the SSC configurations (carbon//carbon (~7 W·h·kg^{-1}), Co_3O_4//Co_3O_4 (~8 W·h·kg^{-1})). Our strategy is very simple, easy to tune, and very suitable for large-scale production. We expect that the convenient method demonstrated by this work could be extended to the development of other metal oxides and carbons with nanoporous structures that are applicable in various research fields.

EXPERIMENTAL METHODS

Materials. We used cobalt(II) chloride, anhydrous (Nacalai Tesque, purity 97%), and 2-methylimidazole (Sigma-Aldrich, purity 99%). Polyvinylpyrrolidone (PVP), hydrochloric acid solution, and methanol were obtained from Nacalai Tesque Reagent Co. All the chemicals were used without any further treatment.

Synthesis of ZIF-67 Polyhedra and Their Conversion into Nanoporous Carbon and Co_3O_4. Synthesis of ZIF-67 is described in our previous report.[50] In brief, in one beaker, $CoCl_2$ (520 mg) and PVP (600 mg) were dissolved in methanol (40 mL) to form a solution. 2-Methylimidazole (2.63 g) was dissolved in methanol (40 mL) to form another clear solution. Then, both solutions were mixed together and stirred for 1 h. This solution was then aged at room temperature, and after 24 h, almost all of the precipitate (purple in color) had settled at the bottom. Then, these powders were washed with methanol and dried for further treatment. A schematic illustration of the synthesis of nanoporous carbon and Co_3O_4 is shown in Scheme 1. Nanoporous carbon was synthesized by direct carbonization of ZIF-67 at 800 °C in nitrogen atmosphere. The temperature of the oven was increased gradually at a heating rate of 5°/min. After the target temperature was reached, these powders were annealed for 5 h and then cooled at room temperature. For the synthesis of Co_3O_4, we tried various heating conditions, such as 350 °C, 400 °C, *etc.* (Figure S7). We found, however, that the optimized heating conditions for obtaining a uniform 3D polyhedral structure of Co_3O_4 are heating in nitrogen atmosphere at 500 °C for 30 min, which prevents collapse of the porous structure. In other cases, however, a very bulky structure was observed. These powders were cooled at room temperature. In addition, the nitrogen supply was turned off, and both ends of the furnace were kept open to heat the sample in air atmosphere at 350 °C for 2 h, resulting in the conversion of these powders to cobalt oxide.

Material Characterization. The morphology of the polyhedral structure was characterized by field emission scanning electron microscopy (Hitachi SU8000) and high-resolution transmission electron microscopy (TECNAI 3010, operated at 200 kV). The crystalline structure of the samples was characterized using powder X-ray diffraction (Rigaku Rint 2500, Cu Kα, $\lambda = 1.5406$ Å). X-ray photoelectron spectroscopy was conducted at room temperature by using a JPS-9010TR (JEOL) instrument with a Mg Kα X-ray source. Nitrogen adsorption−desorption isotherm data were obtained using a BELSORP-mini (BEL, Japan) at 77 K.

Electrochemical Measurements. The electrochemical measurements were performed at room temperature using two- and three-electrode assemblies. The working electrodes were prepared by dispersing the active electrode material (80%) with poly(vinylidene difluoride) (20%) in *N*-methyl 2-pyrrolidinone solvent. The resultant slurry was then coated on graphite substrates and dried at 60 °C for 12 h. For the ASC test, the charge (*Q*) on both the electrodes is balanced by the equation $Q = C \times V \times m$, where *C* is specific capacitance, *V* is the operating potential window, and *m* is mass of the active electrode material. For the SSC and ASC cells, the total mass loading on both the electrodes was 2 $mg \cdot cm^{-2}$. A two-electrode cell consisting of a positive electrode and a negative electrode with a distance of 0.5 cm was used to test the electrochemical properties of the ASC cell in an aqueous KOH electrolyte. The cyclic voltammograms and galvanostatic charge−discharge curves were collected using an electrochemical workstation (CHI 660E, CH Instruments, USA). The specific capacitance ($F \cdot g^{-1}$), specific energy ($W \cdot h \cdot kg^{-1}$), and specific power ($W \cdot kg^{-1}$) were measured per our previous report.[9]

Conflict of Interest: The authors declare no competing financial interest.

Supporting Information Available: Detailed discussions and characterizations of nanoporous carbon and nanoporous Co_3O_4. The Supporting Information is available free of charge on the ACS Publications website at DOI: 10.1021/acsnano.5b01790.

REFERENCES AND NOTES

1. Dai, L. Functionalization of Graphene for Efficient Energy Conversion and Storage. *Acc. Chem. Res.* **2013**, *46*, 31–42.
2. Simon, P.; Gogotsi, Y. Capacitive Energy Storage in Nanostructured Carbon-Electrolyte Systems. *Acc. Chem. Res.* **2013**, *46*, 1094–1103.
3. David, L.; Bhandavat, R.; Singh, G. MoS_2/Graphene Composite Paper for Sodium-Ion Battery Electrodes. *ACS Nano* **2014**, *8*, 1759–1770.
4. Pramanik, M.; Tsujimoto, Y.; Malgras, V.; Dou, S. X.; Kim, J. H.; Yamauchi, Y. Mesoporous Iron Phosphonate Electrodes with Crystalline Frameworks for Lithium-Ion Batteries. *Chem. Mater.* **2015**, *27*, 1082–1089.
5. Salunkhe, R. R.; Lee, Y. H.; Chang, K. H.; Li, J. M.; Simon, P.; Tang, J.; Torad, N. L.; Hu, C. C.; Yamauchi, Y. Nanoarchitectured Graphene-Based Supercapacitors for Next-Generation Energy-Storage Applications. *Chem.—Eur. J.* **2014**, *20*, 13838–13852.
6. Zhang, L. L.; Zhao, X. S. Carbon-Based Materials as Supercapacitor Electrodes. *Chem. Soc. Rev.* **2009**, *38*, 2520–2531.
7. Salunkhe, R. R.; Kamachi, Y.; Torad, N. L.; Hwang, S. M.; Sun, Z.; Dou, S. X.; Kim, J. H.; Yamauchi, Y. Fabrication of Symmetric Supercapacitors Based on MOF-Derived Nanoporous Carbons. *J. Mater. Chem. A* **2014**, *2*, 19848–19854.
8. An, K. H.; Kim, W. S.; Park, Y. S.; Moon, J. M.; Bae, D. J.; Lim, S. C.; Lee, Y. S.; Lee, Y. H. Electrochemical Properties of High-Power Supercapacitors Using Single-Walled Carbon Nanotube Electrodes. *Adv. Funct. Mater.* **2001**, *11*, 387–392.
9. Salunkhe, R. R.; Lin, J.; Malgras, V.; Dou, S. X.; Kim, J. H.; Yamauchi, Y. Large-Scale Synthesis of Coaxial Carbon Nanotube/$Ni(OH)_2$ Composites for Asymmetric Supercapacitor Application. *Nano Energy* **2015**, *11*, 211–218.
10. Fan, Z.; Yan, J.; Wei, T.; Zhi, L.; Ning, G.; Li, T.; Wei, F. Asymmetric Supercapacitors Based on Graphene/MnO_2 and Activated Carbon Nanofiber Electrodes with High Power and Energy Density. *Adv. Funct. Mater.* **2011**, *21*, 2366–2375.
11. Bastakoti, B. P.; Huang, H. S.; Chen, L. C.; Wu, K. C. W.; Yamauchi, Y. Block Copolymer Assisted Synthesis of Porous α-$Ni(OH)_2$ Microflowers with High Surface Areas as Electrochemical Pseudocapacitor Materials. *Chem. Commun.* **2012**, *48*, 9150–9152.
12. Patil, U. M.; Salunkhe, R. R.; Gurav, K. V.; Lokhande, C. D. Chemically Deposited Nanocrystalline NiO Thin Films for Supercapacitor Application. *Appl. Surf. Sci.* **2008**, *255*, 2603–2607.
13. Pérez, C. R.; Yeon, S. H.; Ségalini, J.; Presser, V.; Taberna, P. L.; Simon, P.; Gogotsi, Y. Structure and Electrochemical Performance of Carbide-Derived Carbon Nanopowders. *Adv. Funct. Mater.* **2013**, *23*, 1081–1089.
14. Huang, Y.; Liang, J.; Chen, Y. An Overview of the Applications of Graphene-Based Materials in Supercapacitors. *Small* **2012**, *8*, 1805–1834.
15. Hu, C. C.; Chang, K. H.; Lin, M. C.; Wu, Y. T. Design and Tailoring of the Nanotubular Arrayed Architecture of Hydrous RuO_2 for Next Generation Supercapacitors. *Nano Lett.* **2006**, *6*, 2690–2695.
16. Wang, H.; Casalongue, H. S.; Liang, Y.; Dai, H. $Ni(OH)_2$ Nanoplates Grown on Graphene as Advanced Electrochemical Pseudocapacitor Materials. *J. Am. Chem. Soc.* **2010**, *132*, 7472–7477.
17. Xia, X.; Tu, J.; Zhang, Y.; Wang, X.; Gu, C.; Zhao, X. B.; Fan, H. J. High-Quality Metal Oxide Core/Shell Nanowire Arrays on Conductive Substrates for Electrochemical Energy Storage. *ACS Nano* **2012**, *6*, 5531–5538.
18. Lu, Q.; Chen, J. G.; Xiao, J. Q. Nanostructured Electrodes for High-Performance Pseudocapacitors. *Angew. Chem., Int. Ed.* **2013**, *52*, 1882–1889.
19. Lokhande, C. D.; Dubal, D. P.; Joo, O. S. Metal Oxide Thin Film Based Supercapacitors. *Curr. Appl. Phys.* **2011**, *11*, 255–270.
20. Faraji, S.; Ani, F. N. Microwave-Assisted Synthesis of Metal Oxide/Hydroxide Composite Electrodes for High Power Supercapacitors: A Review. *J. Power Sources* **2014**, *263*, 338–360.
21. Gomez, J.; Kalu, E. E. High-Performance Binder-Free Co-Mn Composite Oxide Supercapacitor Electrode. *J. Power Sources* **2013**, *230*, 218–224.
22. Brezesinski, T.; Wang, J.; Tolbert, S. H.; Dunn, B. Ordered Mesoporous α-MoO_3 with Iso-Oriented Nanocrystalline Walls for Thin-Film Pseudocapacitors. *Nat. Mater.* **2010**, *9*, 146–151.
23. Rauda, I. E.; Augustyn, V.; Dunn, B.; Tolbert, S. H. Enhancing Pseudocapacitive Charge Storage in Polymer Templated Mesoporous Materials. *Acc. Chem. Res.* **2013**, *46*, 1113–1124.
24. Salunkhe, R. R.; Bastakoti, B. P.; Hsu, C. T.; Suzuki, N.; Kim, J. H.; Dou, S. X.; Hu, C. C.; Yamauchi, Y. Direct Growth of Cobalt Hydroxide Rods on Nickel Foam and Its Application for Energy Storage. *Chem.—Eur. J.* **2014**, *20*, 3084–3088.
25. Xia, X. H.; Tu, J. P.; Zhang, Y. Q.; Mai, Y. J.; Wang, X. L.; Gu, C. D.; Zhao, X. B. Freestanding Co_3O_4 Nanowire Array for High Performance Supercapacitors. *RSC Adv.* **2012**, *2*, 1835–1841.
26. Lou, X. W.; Deng, D.; Lee, J. Y.; Feng, J.; Archer, L. A. Self-Supported Formation of Needlelike Co_3O_4 Nanotubes and Their Application as Lithium-Ion Battery Electrodes. *Adv. Mater.* **2008**, *20*, 258–262.
27. Wang, D.; Wang, Q.; Wang, T. Morphology-Controllable Synthesis of Cobalt Oxalates and Their Conversion to Mesoporous Co_3O_4 Nanostructures for Application in Supercapacitors. *Inorg. Chem.* **2011**, *50*, 6482–6492.
28. Cui, L.; Li, J.; Zhang, X. G. Preparation and Properties of Co_3O_4 Nanorods as Supercapacitor Material. *J. Appl. Electrochem.* **2009**, *39*, 1871–1876.
29. Wang, Y.; Zhong, Z.; Chen, Y.; Ng, C. T.; Lin, J. Controllable Synthesis of Co_3O_4 from Nanosize to Microsize with Large-Scale Exposure of Active Crystal Planes and Their Excellent Rate Capability in Supercapacitors Based on the Crystal Plane Effect. *Nano Res.* **2011**, *4*, 695–704.
30. Xiong, S.; Yuan, C.; Zhang, X.; Xi, B.; Qian, Y. Controllable Synthesis of Mesoporous Co_3O_4 Nanostructures with

Tunable Morphology for Application in Supercapacitors. *Chem.—Eur. J.* **2009**, *15*, 5320–5326.
31. Meher, S. K.; Rao, G. R. Ultralayered Co_3O_4 for High-Performance Supercapacitor Applications. *J. Phys. Chem. C* **2011**, *115*, 15646–15654.
32. Wang, H.; Zhang, L.; Tan, X.; Holt, C. M. B.; Zahiri, B.; Olsen, B. C.; Mitlin, D. Supercapacitive Properties of Hydrothermally Synthesized Co_3O_4 Nanostructures. *J. Phys. Chem. C* **2011**, *115*, 17599–17605.
33. Furukawa, H.; Miller, M. A.; Yaghi, O. M. Independent Verification of the Saturation Hydrogen Uptake in MOF-177 and Establishment of a Benchmark for Hydrogen Adsorption in Metal–Organic Frameworks. *J. Mater. Chem.* **2007**, *17*, 3197–3204.
34. Lee, J.; Farha, O. K.; Roberts, J.; Scheidt, K. A.; Nguyen, S. T.; Hupp, J. T. Metal–Organic Framework Materials as Catalysts. *Chem. Soc. Rev.* **2009**, *38*, 1450–1459.
35. Zou, F.; Hu, X.; Li, Z.; Qie, L.; Hu, C.; Zeng, R.; Jiang, Y.; Huang, Y. MOF-Derived Porous ZnO/$ZnFe_2O_4$/C Octahedra with Hollow Interiors for High-Rate Lithium-Ion Batteries. *Adv. Mater.* **2014**, *26*, 6622–6628.
36. Hsu, S. H.; Li, C. T.; Chien, H. T.; Salunkhe, R. R.; Suzuki, N.; Yamauchi, Y.; Ho, K. C.; Wu, K. C. W. Platinum-Free Counter Electrode Comprised of Metal–Organic-Framework (MOF)-Derived Cobalt Sulfide Nanoparticles for Efficient Dye-Sensitized Solar Cells (DSSCs). *Sci. Rep.* **2014**, *4*, No. 6983.
37. Maiti, S.; Pramanik, A.; Mahanty, S. Extraordinarily High Pseudocapacitance of Metal Organic Framework Derived Nanostructured Cerium Oxide. *Chem. Commun.* **2014**, *50*, 11717–11720.
38. Chen, S.; Xue, M.; Li, Y.; Pan, Y.; Zhu, L.; Zhang, D.; Fang, Q.; Qiu, S. Porous $ZnCo_2O_4$ Nanoparticles Derived from a New Mixed-Metal Organic Framework for Supercapacitors. *Inorg. Chem. Front.* **2015**, *2*, 177–183.
39. Kim, T. K.; Lee, K. J.; Cheon, J. Y.; Lee, J. H.; Joo, S. H.; Moon, H. R. Nanoporous Metal Oxides with Tunable and Nanocrystalline Frameworks *via* Conversion of Metal–Organic Frameworks. *J. Am. Chem. Soc.* **2013**, *135*, 8940–8946.
40. Huang, G.; Zhang, F.; Zhang, L.; Du, X.; Wang, J.; Wang, L. Hierarchical $NiFe_2O_4$/Fe_2O_3 Nanotubes Derived from Metal Organic Frameworks for Superior Lithium Ion Battery Anodes. *J. Mater. Chem. A* **2014**, *2*, 8048–8053.
41. Xu, X.; Cao, R.; Jeong, S.; Cho, J. Spindle-like Mesoporous α-Fe_2O_3 Anode Material Prepared from MOF Template for High-Rate Lithium Batteries. *Nano Lett.* **2012**, *12*, 4988–4991.
42. Liu, B.; Shioyama, H.; Akita, T.; Xu, Q. Metal–Organic Framework as a Template for Porous Carbon Synthesis. *J. Am. Chem. Soc.* **2008**, *130*, 5390–5391.
43. Yan, X.; Li, X.; Yan, Z.; Komarneni, S. Porous Carbons Prepared by Direct Carbonization of MOFs for Supercapacitors. *Appl. Surf. Sci.* **2014**, *308*, 306–310.
44. Liu, B.; Shioyama, H.; Jiang, H.; Zhang, X.; Xu, Q. Metal–Organic Framework (MOF) as a Template for Syntheses of Nanoporous Carbons as Electrode Materials for Supercapacitor. *Carbon* **2010**, *48*, 456–463.
45. Amali, A. J.; Sun, J. K.; Xu, Q. From Assembled Metal–Organic Framework Nanoparticles to Hierarchically Porous Carbon for Electrochemical Energy Storage. *Chem. Commun.* **2014**, *50*, 1519–1522.
46. Wu, R.; Wang, D. P.; Han, J.; Liu, H.; Zhou, K.; Huang, Y.; Xu, R.; Wei, J.; Chen, X.; Chen, Z. A General Approach towards Multi-faceted Hollow Oxide Composites Using Zeolitic Imidazolate Frameworks. *Nanoscale* **2015**, *7*, 965–974.
47. Morozan, A.; Jaouen, F. Metal–Organic Frameworks for Electrochemical Applications. *Energy Environ. Sci.* **2012**, *5*, 9269–9290.
48. Ma, T. Y.; Dai, S.; Jaroniec, M.; Qiao, S. Z. Metal–Organic Framework Derived Hybrid Co_3O_4-Carbon Porous Nanowire Arrays as Reversible Oxygen Evolution Electrodes. *J. Am. Chem. Soc.* **2014**, *136*, 13925–13931.
49. Wu, R.; Qian, X.; Zhou, K.; Wei, J.; Lou, J.; Ajayan, P. M. Porous Spinel $Zn_xCo_{(3-x)}O_4$ Hollow Polyhedra Templated for High-Rate Lithium-Ion Batteries. *ACS Nano* **2014**, *8*, 6297–6303.
50. Torad, N. L.; Salunkhe, R. R.; Li, Y.; Hamoudi, H.; Imura, M.; Sakka, Y.; Hu, C. C.; Yamauchi, Y. Electric Double-Layer Capacitors Based on Highly Graphitized Nanoporous Carbons Derived from ZIF-67. *Chem.—Eur. J.* **2014**, *20*, 7895–7900.
51. Tang, C. H.; Yin, X.; Gong, H. Superior Performance Asymmetric Supercapacitors Based on a Directly Grown Commercial Mass 3D Co_3O_4@$Ni(OH)_2$ Core–Shell Electrode. *ACS Appl. Mater. Interfaces* **2013**, *5*, 10574–10582.
52. Zhang, F.; Hao, L.; Zhang, L.; Zhang, X. Solid-State Thermolysis Preparation of Co_3O_4 Nano/Micro Superstructures from Metal–Organic Framework for Supercapacitors. *Int. J. Electrochem. Sci.* **2011**, *6*, 2943–2954.
53. Yang, K.; Gu, M.; Guo, Y.; Pan, X.; Mu, G. Effects of Carbon Nanotube Functionalization on the Mechanical and Thermal Properties of Epoxy Composites. *Carbon* **2009**, *47*, 1723–1737.
54. Tang, J.; Salunkhe, R. R.; Liu, J.; Torad, N. L.; Imura, M.; Furukawa, S.; Yamauchi, Y. Thermal Conversion of Core–Shell Metal–Organic Frameworks: A New Method for Selectively Functionalized Nanoporous Hybrid Carbon. *J. Am. Chem. Soc.* **2015**, *137*, 1572–1580.
55. Armelao, L.; Barreca, D.; Gross, S.; Tondello, E. Sol–Gel and CVD Co_3O_4 Thin Films Characterized by XPS. *Surf. Sci. Spectra* **2001**, *8*, 14–23.
56. Wang, X.; Li, M.; Chang, Z.; Yang, Y.; Wu, Y.; Liu, X. Co_3O_4@MWCNT Nanocable as Cathode with Superior Electrochemical Performance for Supercapacitors. *ACS Appl. Mater. Interfaces* **2015**, *7*, 2280–2285.
57. Tang, Z.; Tang, C. H.; Gong, H. A High Energy Density Asymmetric Supercapacitor from Nano-Architectured $Ni(OH)_2$/Carbon Nanotube Electrodes. *Adv. Funct. Mater.* **2012**, *22*, 1272–1278.
58. Peng, Y. J.; Wu, T. H.; Hsu, C. T.; Li, S. M.; Chen, M. G.; Hu, C. C. Electrochemical Characteristics of the Reduced Graphene Oxide/Carbon Nanotube/Polypyrrole Composites for Aqueous Asymmetric Supercapacitors. *J. Power Sources* **2014**, *272*, 970–978.
59. Li, H. B.; Yu, M. H.; Wang, F. X.; Liu, P.; Liang, Y.; Xiao, J.; Wang, C. X.; Tong, Y. X.; Yang, G. W. Amorphous Nickel Hydroxide Nanospheres with Ultrahigh Capacitance and Energy Density as Electrochemical Pseudocapacitor Materials. *Nat. Commun.* **2013**, *4*, 1894.